# The physics of hadron radiotherapy

Author: Ona Pérez Prades
*Facultat de Física, Universitat de Barcelona, Diagonal 645, 08028 Barcelona, Spain*

Advisor: José M. Fernández-Varea
(Dated: January 2023)

**Abstract:** The use of hadron beams in radiotherapy is rapidly increasing as they present numerous advantages in treating deep-seated tumors. The purpose of this TFG is to give an overview of the physics behind radiotherapeutic hadron beams, especially for $^{1}H^{+}$ and $^{12}C^{6+}$ ions. This study reviews the basic aspects of the physics of hadron therapy, including slowing down processes, hadron interaction mechanisms and hadron depth-dose curves, through analytical calculations.

## I. INTRODUCTION

Radiotherapy is one of the three main cancer treatment modalities, along with chemotherapy and surgery. According to the Spanish Society of Radiotherapeutic Oncology, about 60% of cancer patients require at least one radiotherapy session as part of their treatment [1]. In radiotherapy, a controlled amount of ionizing radiation is aimed at a particular part of the body to treat a disease, which is generally a malignant tumor. Ideally, the planned target volume should receive 100% of the absorbed dose prescribed to kill cancer cells while minimizing the damage to the surrounding healthy tissues. There are mainly two types of radiotherapy, namely brachytherapy and external-beam radiotherapy. The latter, which is the most common type of radiotherapy and the one reviewed in this study, involves directing ionizing radiation to the patient's tumor location from a distant source. The absorbed dose is usually delivered by beams of electrons or x-rays. MeV electrons are convenient for treating tumors located near the surface of the body, whereas MV x-rays are better for dealing with deeper tumors. However, these radiation qualities have some inconveniences. Electrons and photons are easily scattered so that organs near the tumor get irradiated. Moreover, electron beams generate Bremsstrahlung photons, which increases the possibility of damaging healthy tissues behind the tumor.

Nowadays, external-beam radiotherapy with hadron beams is increasing owing to their advantages over the aforementioned beams. Hadron beams are characterized by more rectilinear trajectories, very low Bremsstrahlung emission, and favorable depth-dose curves. Moreover, hadrons are more lethal to cancer cells because of their high linear-energy-transfer (related to the electronic stopping power), as they damage the cells' DNA enhancing the yield of double-strand breaks, which cancer cells are not able to repair. $^{1}$H and $^{12}$C ion beams are two examples of hadron beams already implemented in oncological clinics. There are approximately 100 proton therapy centres and 13 carbon ion therapy centres operating worldwide [2, 3]. Other hadrons, such as $^{3}$He and $^{4}$He ions, are currently being investigated for potential future usage.

The aim of this work is to explore the benefits of using hadron beams in cancer treatment. Concretely, the beams that have been extensively analyzed and reviewed have been $^{1}H^{+}$, $^{4}He^{2+}$ and $^{12}C^{6+}$ beams.

The report is divided into three sections. The first one focuses on how the ion beam loses energy due to the electromagnetic interactions with the electrons in the medium, the second one addresses the probability of nuclear reactions through the study of their reaction cross sections, and finally, the third one focuses on the beam's depth-fluence and depth-dose curves. In order to perform the analytical calculations, a few Fortran90 programs have been developed. We have also compared the results of this study with experimental measurements and data from ICRU Report 90.

## II. ENERGY LOSS

One of the main advantages of hadron beams is how they lose energy along their trajectories. The topic addressed in this section is the electronic stopping power because in the case of hadron beams the nuclear and radiative stopping powers are negligible. The nuclear stopping power becomes appreciable at very low energies ($\leq$ 1 MeV). The radiative stopping power, which quantifies the energy loss due to the emission of Bremsstrahlung photons, is almost null since it is proportional to $M^{-2}$, where $M$ is the mass of the projectile charged particle. In fact, the only Bremsstrahlung radiation that is emitted comes from secondary electrons ejected in inelastic collisions.

### A. Mass electronic stopping power

The electronic stopping power is defined as the energy loss experienced by charged particles per unit path length due to inelastic collisions with the electrons of the medium. The mass electronic stopping power has been calculated according to the relativistic Bethe–Bloch formula used in ICRU Report 90 [4]

$$S_{el}/\rho = \frac{Z_1^2 Z_2}{\beta^2 A_2}\, C_0^{HCP} \left[L_0 + Z_1\, L_1 + Z_1^2\, L_2\right], \quad (1)$$

where $C_0^{HCP} = 0.307075$ MeV cm$^2$/g, $Z_1$ is the charge of the projectile and $Z_2$ is the atomic number of the absorbing material, which has been considered liquid water as a first approximation. Since $L_0 \gg Z_1 L_1 > Z_1^2 L_2$, the terms $Z_1 L_1$ (Barkas–Andersen correction) and $Z_1^2 L_2$ (Bloch correction) have been neglected. The dominant term $L_0$, which is the relativistic Bethe stopping number, is given by

$$L_0 = \ln\left(\frac{2m_e c^2(\beta\gamma)^2}{I}\right) - \beta^2 - \frac{C(\beta)}{Z_2} - \frac{\delta(\gamma)}{2}, \qquad (2)$$

where $I$ is the mean excitation energy of the absorbing material ($I = 78$ eV for liquid water), $C(\beta)/Z_2$ is the shell correction and $\delta(\gamma)$ is the density-effect correction. The shell correction is significant only at very low energies and the density effect is appreciable at very high energies. Therefore, the $C/Z_2$ and $\delta$ terms have been omitted because they are negligible in the energy range of present concern, which spans from a few MeV/N to several hundred MeV/N.

Figure 1 shows the mass electronic stopping powers of liquid water calculated with the simplified Bethe–Bloch formula adopted here and the values tabulated in ICRU Report 90. The large differences visible at low energies are due to the neglect of the shell, Barkas–Andersen and Bloch corrections. However, in the therapeutic energy interval the agreement between the simplified and complete versions of the Bethe–Bloch formula is almost perfect. The electronic stopping power is large at low energies. This means that towards the end of their trajectories the ions of the beam are stopped quicker, resulting in the deposition of a larger energy, and therefore absorbed dose. In addition, it can be observed that the stopping power is larger for heavier ions, which means that a higher initial kinetic energy is required in order to penetrate the same depth in the body.

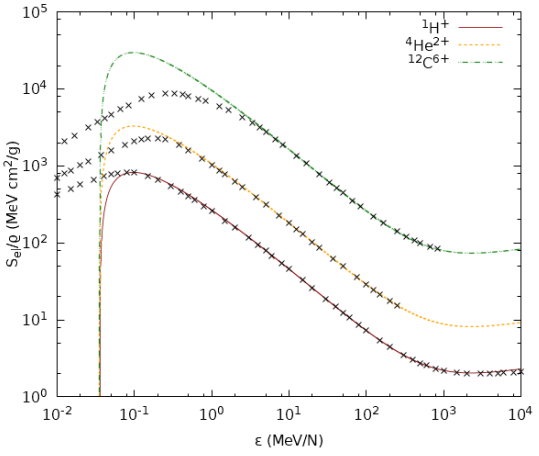


FIG. 1: Mass electronic stopping power versus ion energy per nucleon for $^1H^+$, $^4He^{2+}$ and $^{12}C^{6+}$ ion beams in liquid water. The black symbols are the corresponding data from ICRU Report 90 [4].

### B. Mass CSDA range

The range is defined as the depth at which the ions of the beam come to rest, so it describes the average length that the beam can penetrate in a medium. The range has been calculated using the continuous-slowing-down-approximation (CSDA), which is based on the assumption that the slowing down of the ions is gradual, i.e. disregarding fluctuations in the energy loss,

$$\rho r_0 \approx \int_0^E \frac{1}{S_{el}(E')/\rho}\, dE'. \qquad (3)$$

The mass CSDA ranges calculated with Eqs. (1)–(3) are displayed in Fig. 2. Although our results differ at low energies from the data recommended by ICRU Report 90, they align closely with them at intermediate and high energies. CSDA ranges are useful to determine the initial energy of the beam that is required to reach a tumor located at a specific depth. Tipically, tumors treated with hadron beams are located at depths up to around 25 cm. To reach these depths, $^1$H and $^4$He ion beams need an initial energy around 200 MeV/N, whereas $^{12}$C ion beams require roughly 400 MeV/N.

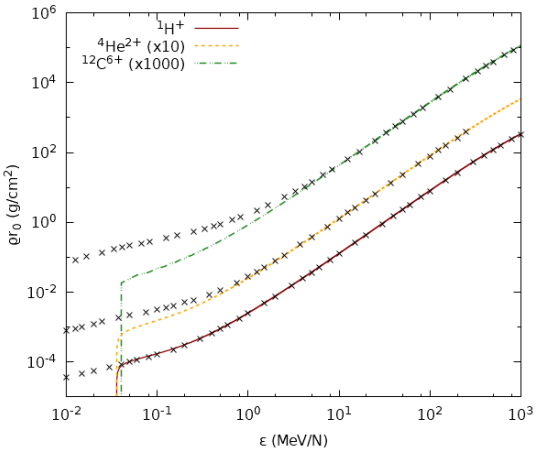


FIG. 2: Mass CSDA range versus ion energy per nucleon for $^1H^+$, $^4He^{2+}$ and $^{12}C^{6+}$ ions in liquid water. The black symbols are values taken from ICRU Report 90 [4]. Notice that the data for $^4He^{2+}$ and $^{12}C^{6+}$ beams have been multiplied by 10 and 1000, respectively.

## III. NUCLEAR REACTIONS

Hadron beams also interact with the atomic nuclei of the body via non-elastic nuclear reactions. While the stopping process of hadron beams is governed by the interactions with atomic electrons, the probability of nuclear reactions is much smaller. However, nuclear reactions lead to significant effects at large penetration depths. The main consequences of nuclear reactions are

a decrease in the absorbed dose due to the removal of ions from the beam and the creation of secondary ions and particles [5]. These secondary particles may introduce a small contribution to the absorbed dose beyond the CSDA range. Although in principle this is a drawback, recent studies suggest that some of the particles generated in nuclear reactions might be utilized to trace the beam direction through PET scans, improving the accuracy of the treatment [6].

To study the probability of nuclear reactions of the hadron beams, we have chosen $^{16}$O nuclei as the target because oxygen represents a 65% of the mass of the human body. We have calculated the reaction cross sections of the $^{1}$H+$^{16}$O, $^{4}$He+$^{16}$O and $^{12}$C+$^{16}$O reactions by means of the semi-empirical model of Kox *et al* [7]

$$\sigma_R = \pi r_0^2 \left[A_P^{1/3} + A_T^{1/3} + S(A_P, A_T) - c(\varepsilon)\right]^2 \times \left(1 - \frac{V_B}{E_{cm}}\right), \quad (4)$$

where the subindices $P$ and $T$ indicate projectile' magnitudes and target' magnitudes, respectively, $r_0 = 1.1$ fm, $V_B$ the Coulomb barrier height, $S(A_P, A_T)$ the mass asymmetry function, and $c(\varepsilon)$ the transparency function. The mass asymmetry function is given by

$$S(A_P, A_T) = a \frac{A_P^{1/3} A_T^{1/3}}{A_P^{1/3} + A_T^{1/3}} \quad (5)$$

with $a = 1.85$. In turn, we have calculated the transparency function c($\varepsilon$) using the parameterization proposed by Sihver *et al* [8]. The Coulomb barrier height $V_B$ has been estimated using Shen *et al*'s model [9]

$$V_B = \frac{Z_P Z_T e^2}{R_B} - b\left(\frac{1}{R_P} + \frac{1}{R_T}\right)^{-1}, \quad (6)$$

where $b = 1$ MeV/fm and the Coulomb barrier position $R_B$ is given by

$$R_B = R_P + R_T + \Delta R \quad (7)$$

with

$$R_i = (1.12 \text{ fm})\, A_i^{1/3} - (0.94 \text{ fm})\, A_i^{-1/3} \quad i = P, T \quad (8)$$

$$\Delta R = 3.2 \text{ fm}. \quad (9)$$

Finally, the non-relativistic kinetic energy in the center-of-mass reference frame is

$$E_{cm} = \varepsilon \left(\frac{1}{A_P} + \frac{1}{A_T}\right)^{-1}. \quad (10)$$

As seen in Fig. 3, the reaction cross section of the three reactions have a similar shape, with a maximum around 10 MeV/N. This means that when the beam has this energy, which happens nearly at the end of its path, is more susceptible to undergo nuclear reactions with $^{16}$O nuclei. It can also be noticed that the reaction cross section at energies of hundreds of MeV/N is almost constant. Additionally, it can be observed that heavier nuclei, such as $^{12}$C ions, have a higher probability of interacting with $^{16}$O nuclei.

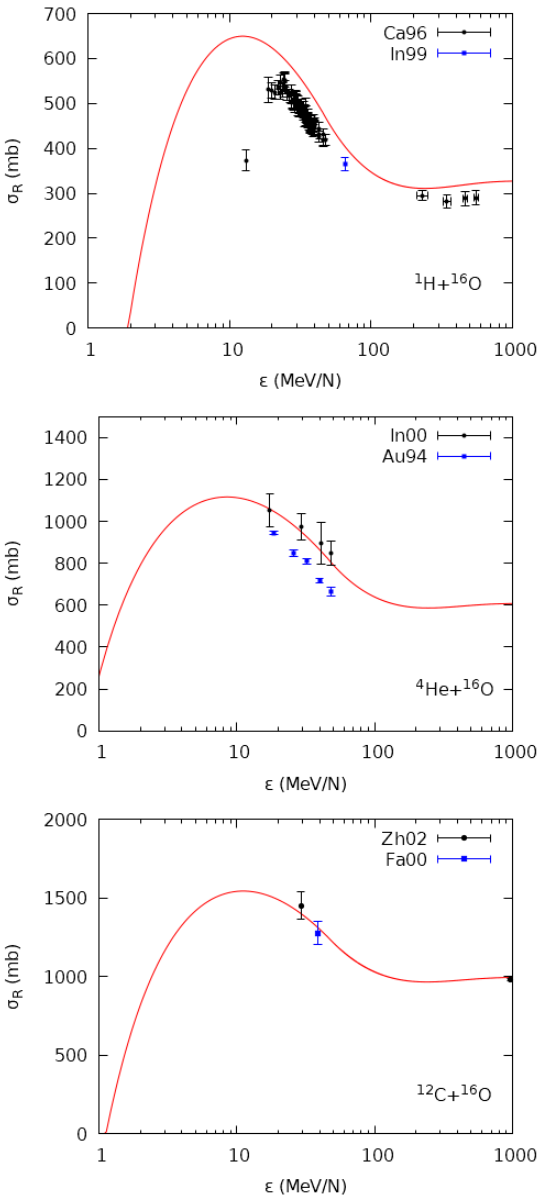


FIG. 3: Nuclear reaction cross section versus energy per nucleon of $^{1}$H, $^{4}$He and $^{12}$C nuclei as projectiles and $^{16}$O nuclei as target. The experimental data are from Ca96 [10], In99 [11], In00 [12], Au94 [13], Zh02 [14] and Fa00 [15].

## IV. FLUENCE AND ABSORBED DOSE

### A. Fluence

Fluence is the number of particles that crosses a unit area, serving to quantify how the beam is attenuated along its path due to nuclear reactions. The fluence has been computed by means of the Beer–Lambert law [16]

$$\Phi(z) = \Phi_0 \exp\left(-\frac{\mu}{\rho}\rho z\right), \tag{11}$$

where $\Phi_0$ is the fluence of the beam at $z = 0$ and the mass attenuation coefficient is

$$\frac{\mu}{\rho} = \frac{N_A\,\sigma_R}{\mathcal{M}}, \tag{12}$$

where $N_A$ is the Avogadro constant, $\mathcal{M}$ is the molar mass of $H_2O$, and $\sigma_R$ is the reaction cross section with $^{16}O$ nuclei. The initial energies $E_0$ of the beams have been determined so that the CSDA ranges were exactly 25 cm. The reaction cross sections have been treated as constants $\sigma_R(E_0)$.

As shown in Fig. 4, $^{12}C^{6+}$ beams lose energy due to nuclear reactions more quickly than proton beams, because its reaction cross section is greater. However, the actual fluence curves are not discontinuous at $r_0$. Instead, they decrease smoothly near the CSDA range due to the fluctuations in the energy loss of the beam.

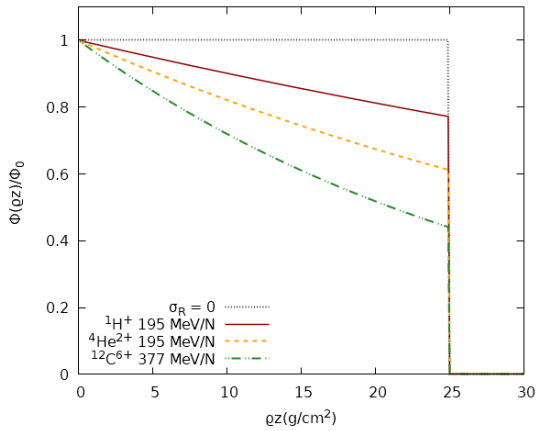


FIG. 4: Relative fluence for $^1H^+$, $^4He^{2+}$ and $^{12}C^{6+}$ beams as a function of the traversed mass thickness $\rho z$.

### B. Absorbed dose

The main reason for using hadron beams in radiotherapy is their favorable depth-dose profile. To represent the depth-dose curves, we compute the absorbed dose of monoenergetic beams [17]

$$\begin{aligned} D(z) &\approx -\frac{1}{\rho}\frac{d}{dz}\big(\Phi(z)E(z)\big) \\ &\approx \Phi(z)\,\frac{S_{el}(z)}{\rho} + E(z)\left(-\frac{1}{\rho}\frac{d\Phi(z)}{dz}\right). \end{aligned} \tag{13}$$

The depth-dose curves have been calculated both taking into account nuclear reactions ($\sigma_R \neq 0$) and neglecting them ($\sigma_R = 0$). As shown in Fig. 5, nuclear reactions are more significant for $^{12}C^{6+}$ beams than for $^1H^+$ beams. Moreover, the depth-dose curves display a prominent peak close to the CSDA range, known as the "Bragg peak". This is a major advantage of hadron radiotherapy, as they deposit most of their energy at the location of the tumor and do not affect organs that are beyond it. However, the actual depth-dose curves have a residual remaining dose after the Bragg peak, the so-called "fragmentation tail". Since $^{12}C^{6+}$ ion beams are more likely to have nuclear reactions, its fragmentation tail is bigger.

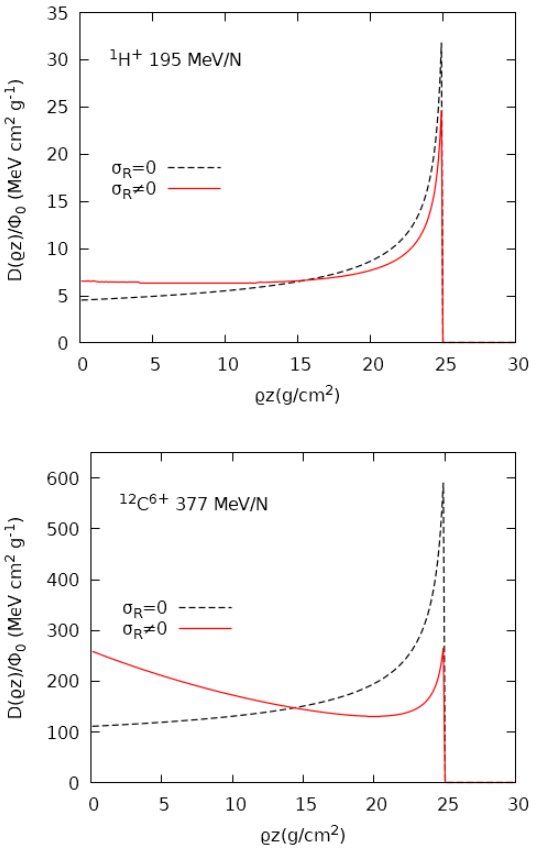


FIG. 5: Depth-dose curves for $^1H^+$ and $^{12}C^{6+}$ ion beams in liquid water. The solid and dashed curves were calculated including or neglecting nuclear reactions, respectively.

Broad "spread-out Bragg peaks" (SOBPs) are created by the superposition of monoenergetic beams with different CSDA ranges that, multiplied by suitable weights, form a nearly uniform dose in the tumor. In Fig. 6,

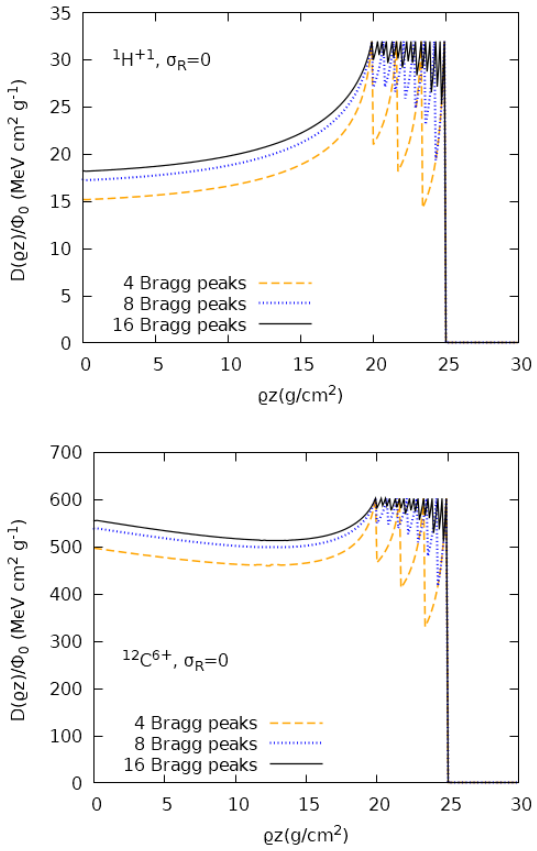


FIG. 6: SOBPs for $^1H^+$ and $^{12}C^{6+}$ beams in liquid water using 4, 8 and 16 beams, covering 20–25 cm depths.

SOBPs were computed for $^1H^+$ and $^{12}C^{6+}$ beams so as to cover a depth range between 20 cm and 25 cm. These SOBPs were generated neglecting nuclear reactions. As we increase the number of beams, the absorbed dose becomes more uniform at the tumor location.

## V. CONCLUSIONS

Hadron radiotherapy is a successful cancer treatment modality that offers many advantages. Hadron beams can be attenuated by two methods: through inelastic collisions with the electrons in the medium, and through nuclear reactions. The combination of these two interaction mechanisms results in a distinct maximum of the absorbed dose at the location of the tumor, preventing the organs and tissues beyond the peak from being irradiated. Therefore, hadron-beam radiotherapy stands as an effective option for cancer treatment, particularly for tumors that are located close to critical organs that would be damaged by traditional radiotherapy techniques.

### Acknowledgments

I would like to express my sincere gratitude to my supervisor, José M. Fernández-Varea, for his guidance, support and advice throughout the elaboration of this work. I also thank my family and friends, who always bring out the best in me, for their constant love and motivation.

[1] R. Arráns et al. *Libro Blanco de la Protonterapia*. Sociedad Andaluza de Radiofísica Hospitalaria, 2021.
[2] F. Aliyah, S. G. Pinasti, and A. A. Rahman. Proton therapy facilities: an overview of the development in recent years. volume 927, 2021.
[3] T. D. Malouff, A. Mahajan, S. Krishnan, et al. Carbon ion therapy: a modern review of an emerging technology. *Frontiers Oncol.*, 10:82, 2020.
[4] S. M. Seltzer et al. Key data for ionizing-radiation dosimetry: measurement standards and applications, ICRU Report 90. 2016.
[5] W. D. Newhauser et al. The physics of proton therapy. *Phys. Med. Biol.*, 60(8):R155, 2015.
[6] D. Schardt, T. Elsässer, et al. Heavy-ion tumor therapy: Physical and radiobiological benefits. *Rev. Mod. Phys.*, 82(1):383, 2010.
[7] S. Kox, A. Gamp, et al. Trends of total reaction cross sections for heavy ion collisions in the intermediate energy range. *Phys. Rev. C*, 35(5):1678, 1987.
[8] L. Sihver et al. Improved parametrization of the transparency parameter in Kox and Shen models of total reaction cross sections. *Phys. Rev. C*, 89(6):067602, 2014.
[9] W. Shen, B. Wang, J. Feng, et al. Total reaction cross section for heavy-ion collisions and its relation to the neutron excess degree of freedom. *Nucl. Phys. A*, 491(1):130–146, 1989.
[10] R. F. Carlson. Proton-nucleus total reaction cross sections and total cross sections up to 1 GeV. *At. Data Nucl. Data Tables*, 63(1):93–116, 1996.
[11] A. Ingemarsson, J. Nyberg, et al. Reaction cross sections for 65 MeV protons on targets from $^9$Be to $^{208}$Pb. *Nucl. Phys. A*, 653(4):341–354, 1999.
[12] A. Ingemarsson et al. New results for reaction cross sections of intermediate energy $\alpha$-particles on targets from $^9$Be to $^{208}$Pb. *Nucl. Phys. A*, 676(1-4):3–31, 2000.
[13] A. Auce, R. F. Carlson, A. J. Cox, et al. Reaction cross sections for 75–190 MeV alpha particles on targets from $^{12}$C to $^{208}$Pb. *Phys. Rev. C*, 50(2):871, 1994.
[14] H. Zhang, W. Shen, et al. Measurement of reaction cross section for proton-rich nuclei (A<30) at intermediate energies. *Nucl. Phys. A*, 707(3-4):303–324, 2002.
[15] D. Fang, W. Shen, J. Feng, et al. Measurements of total reaction cross sections for some light nuclei at intermediate energies. *Phys. Rev. C*, 61(6):064311, 2000.
[16] M. Lazzeroni. *Production of high quality $^{11}$C beams for radiation treatment and accurate PET-CT dose delivery verification.* PhD thesis, 2013.
[17] T. Bortfeld. An analytical approximation of the Bragg curve for therapeutic proton beams. *Med. Phys.*, 24(12):2024–2033, 1997.

## ANNEX

Here we collect additional reaction cross sections, calculated during the development of this project, for $^{12}$C and $^{14}$N target nuclei. Recall that, together with oxygen, carbon and nitrogen atoms are among the most abundant atomic species in the human body.

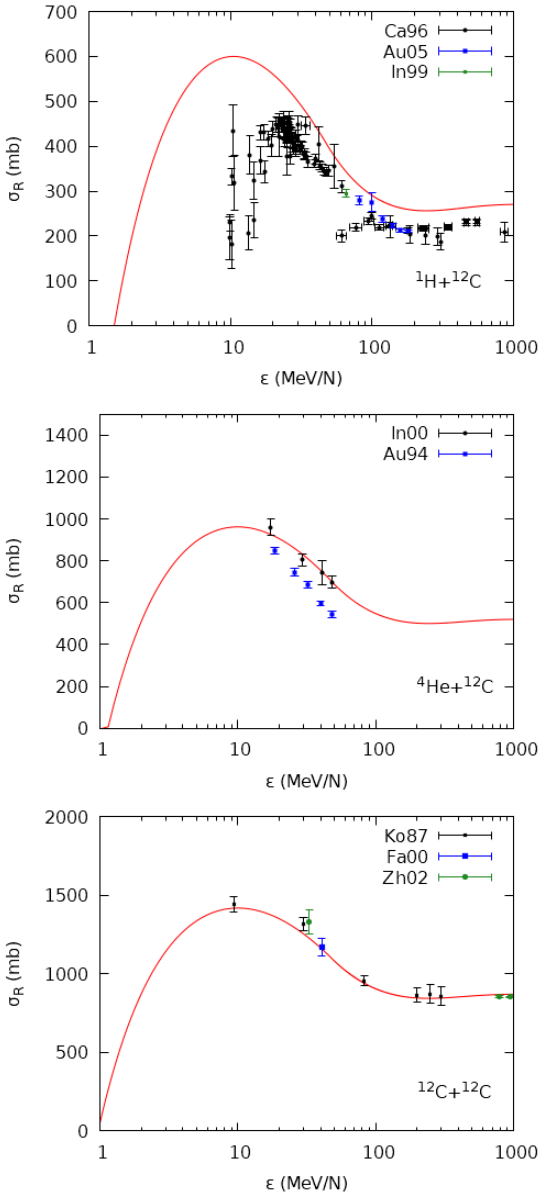


FIG. 7: Reaction cross sections versus energy per nucleon for $^{1}$H, $^{4}$He and $^{12}$C nuclei as projectiles and $^{12}$C nuclei as target. The experimental data are from references Ca96 [10], Au05 [Au05], In99[11], In00 [12], Au94 [13], Ko87[7], Fa00 [15] and Zh02 [14].

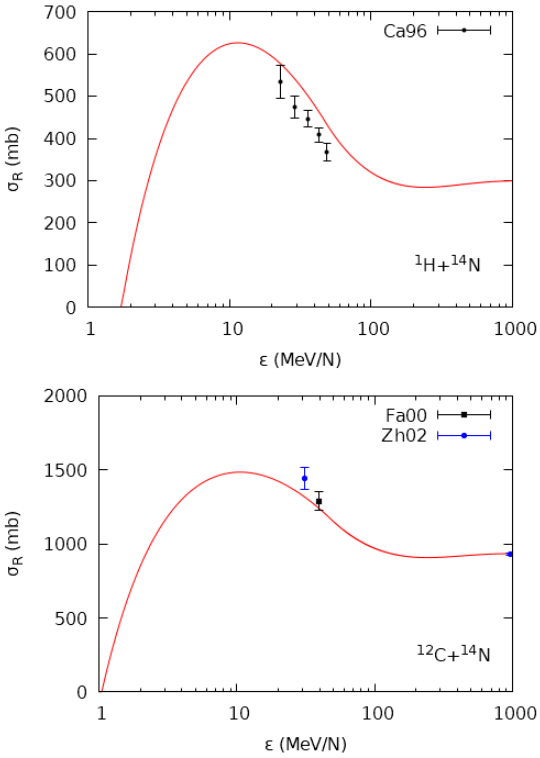


FIG. 8: Reaction cross sections versus energy per nucleon for $^{1}$H and $^{12}$C nuclei as projectiles and $^{14}$N nuclei as target. The experimental data are from references Ca96 [10], Fa00 [15] and Zh02 [14].

[Au05] A. Auce, *et. al.* Reaction cross sections for protons on $^{12}$C,$^{40}$ Ca,$^{90}$ Zr, and $^{208}$Pb at energies between 80 and 180 MeV. *Phys. Rev. C*, 71(6):064606, 2005.